SOLUTIONS OF INVISCID AND VISCOUS FLOWS USING STRUCTURED HIGH RESOLUTION ALGORITHMS IN THREE-DIMENSIONS

Edisson Sávio de Góes Maciel*
***Researcher, Rua Demócrito Cavalcanti, 152, Afogados, Recife, PE, Brazil, 50750-080**
edissonsavio@yahoo.com.br

Keywords: *Yee, Warming and Harten algorithm, Hughson and Beran algorithm, Cebeci and Smith model, Baldwin and Lomax model, Euler and Navier-Stokes equations.*

Abstract

The present work performs comparisons between the Yee, Warming and Harten and the Hughson and Beran algorithms in the solution of inviscid and laminar and turbulent viscous flows in three-dimensions. The Euler and the Navier-Stokes equations, on a finite volume context and using a structured spatial discretization, are solved. The algorithms are flux difference splitting type and a dimensional splitting method is used to perform time integration. The physical problem of the supersonic flow along a ramp is studied. Turbulence is taking into account considering two turbulence models, namely: the Cebeci and Smith and the Baldwin and Lomax algebraic ones. The results have demonstrated that the Hughson and Beran scheme yields more severe pressure fields, while the Yee, Warming and Harten scheme presents more accurate results.

1 Introduction

Conventional non-upwind algorithms have been used extensively to solve a wide variety of problems (Kutler [1] and Steger [2]). Conventional algorithms are somewhat unreliable in the sense that for every different problem (and sometimes, every different case in the same class of problems) artificial dissipation terms must be specially tuned and judicially chosen for convergence.

Upwind schemes are in general more robust but are also more involved in their derivation and application. Some upwind schemes that have been applied to the Euler equations are: Yee, Warming and Harten [3], and Hughson and Beran [4]. Some comments about these methods are reported below:

Yee, Warming and Harten [3] implemented a high resolution second order explicit method based on Harten's ideas. The method had the following properties: (a) the scheme was developed in conservation form to ensure that the limit was a weak solution; (b) the scheme satisfied a proper entropy inequality to ensure that the limit solution would have only physically relevant discontinuities. The method was applied to the solution of a quasi-one-dimensional nozzle problem and to the two-dimensional shock reflection problem, yielding good results.

Hughson and Beran [4] proposed an explicit, second order accurate in space, TVD (Total Variation Diminishing) scheme to solve the Euler equations in axis-symmetrical form, applied to the studies of the supersonic flow around a sphere and the hypersonic flow around a blunt body. The scheme was based on the modified flux function approximation of Harten [5] and its extension from the two-dimensional space to the axis-symmetrical treatment was developed. Results were of good quality.

There is a practical necessity in the aeronautical industry and in other fields of the capability of calculating separated turbulent compressible flows. With the available numerical methods, researches seem able to analyze several separated flows, three-dimensional in general, if an appropriated turbulence model is employed. Simple methods, as the algebraic turbulence models of Cebeci and Smith [6] and of Baldwin and Lomax [7], supply satisfactory results with low computational cost.

The present work performs comparisons between the Yee, Warming and Harten [3] and the Hughson and Beran [4] algorithms in the solution of inviscid and laminar and turbulent viscous flows in three-dimensions. The Euler and the Navier-Stokes equations, on a finite volume context and using a structured spatial discretization, are solved. The algorithms to perform numerical experiments are of TVD flux difference splitting type, second order accurate. A dimensional splitting method, first order accurate, is used to time integration. The physical problem of the supersonic flow along a ramp is studied. Turbulence is taking into account considering two turbulence models, namely: the Cebeci and Smith [6] and the Baldwin and Lomax [7] algebraic ones. The results have demonstrated that the Hughson and Beran [4] yields more severe pressure fields, while the Yee, Warming and Harten [3] scheme presents more accurate results.

2 Navier-Stokes Equations

As the Euler equations can be obtained from the Navier-Stokes ones by disregarding the viscous vectors, only the formulation to the later will be presented. The Navier-Stokes equations in integral conservative form, employing a finite volume formulation and using a structured spatial discretization, to three-dimensional simulations, can be written as:

$$\partial Q/\partial t + 1/V\int_V \vec{\nabla}\cdot\vec{P}\,dV = 0\,, \qquad (1)$$

where V is the cell volume, which corresponds to an hexahedron in the three-dimensional space; Q is the vector of conserved variables; and $\vec{P} = (E_e - E_v)\vec{i} + (F_e - F_v)\vec{j} + (G_e - G_v)\vec{k}$ represents the complete flux vector in Cartesian coordinates, with the subscript "e" related to the Euler contributions and "v" is related to the viscous contributions. These vectors are described below:

$$Q = \begin{Bmatrix} \rho \\ \rho u \\ \rho v \\ \rho w \\ e \end{Bmatrix},\; E_e = \begin{Bmatrix} \rho u \\ \rho u^2 + p \\ \rho uv \\ \rho uw \\ (e+p)u \end{Bmatrix},\; F_e = \begin{Bmatrix} \rho v \\ \rho uv \\ \rho v^2 + p \\ \rho vw \\ (e+p)v \end{Bmatrix}, \qquad (2)$$

$$G_e = \begin{Bmatrix} \rho w \\ \rho uw \\ \rho vw \\ \rho w^2 + p \\ (e+p)w \end{Bmatrix},\; E_v = \frac{1}{\mathrm{Re}}\begin{Bmatrix} 0 \\ \tau_{xx} \\ \tau_{xy} \\ \tau_{xz} \\ \tau_{xx}u + \tau_{xy}v + \tau_{xz}w - q_x \end{Bmatrix}, \qquad (3)$$

$$F_v = \frac{1}{\mathrm{Re}}\begin{Bmatrix} 0 \\ \tau_{yx} \\ \tau_{yy} \\ \tau_{yz} \\ \tau_{yx}u + \tau_{yy}v + \tau_{yz}w - q_y \end{Bmatrix},\; G_v = \frac{1}{\mathrm{Re}}\begin{Bmatrix} 0 \\ \tau_{zx} \\ \tau_{zy} \\ \tau_{zz} \\ \tau_{zx}u + \tau_{zy}v + \tau_{zz}w - q_z \end{Bmatrix}. \qquad (4)$$

In these equations, the components of the viscous stress tensor are defined as:

$$\tau_{xx} = 2(\mu_M + \mu_T)\partial u/\partial x - 2/3(\mu_M + \mu_T)(\partial u/\partial x + \partial v/\partial y + \partial w/\partial z); \quad (5)$$

$$\tau_{xy} = (\mu_M + \mu_T)(\partial u/\partial y + \partial v/\partial x), \tau_{xz} = (\mu_M + \mu_T)(\partial u/\partial z + \partial w/\partial x); \quad (6)$$

$$\tau_{yy} = 2(\mu_M + \mu_T)\partial v/\partial y - 2/3(\mu_M + \mu_T)(\partial u/\partial x + \partial v/\partial y + \partial w/\partial z); \quad (7)$$

$$\tau_{yz} = (\mu_M + \mu_T)(\partial v/\partial z + \partial w/\partial y) \text{ and} \qquad (8)$$

$$\tau_{zz} = 2(\mu_M + \mu_T)\partial w/\partial z - 2/3(\mu_M + \mu_T)(\partial u/\partial x + \partial v/\partial y + \partial w/\partial z). \quad (9)$$

The components of the conductive heat flux vector are defined as follows:

$$q_x = -\gamma(\mu_M/\mathrm{Pr}\,d + \mu_T/\mathrm{Pr}\,d_T)\partial e_i/\partial x; \qquad (10)$$

$$q_y = -\gamma(\mu_M/\mathrm{Pr}\,d + \mu_T/\mathrm{Pr}\,d_T)\partial e_i/\partial y; \qquad (11)$$

$$q_z = -\gamma(\mu_M/\mathrm{Pr}\,d + \mu_T/\mathrm{Pr}\,d_T)\partial e_i/\partial z. \qquad (12)$$

The quantities that appear above are described as follows: ρ is the fluid density, u, v and w are the Cartesian components of the flow velocity vector in the x, y and z directions, respectively; e is the total energy; p is the fluid static pressure; e_i is the fluid internal energy; the τ's represent the components of the viscous stress tensor; Prd is the laminar Prandtl number (=0.72); Prd_T is the turbulent Prandtl number (=0.9); the q's represent the components of the conductive heat flux; μ_M is the fluid molecular viscosity; μ_T is the fluid turbulent viscosity; γ is the ratio of specific heats at constant pressure and volume, respectively (=1.4); and Re is the Reynolds number of the simulation. The molecular viscosity is estimated by the Sutherland law.

The Navier-Stokes equations were nondimensionalized in relation to freestream properties. To allow the solution of the matrix system of five equations to five unknowns defined by Eq. (1), it is used the state equation:

$$p = (\gamma - 1)\left[e - 0.5\rho(u^2 + v^2 + w^2)\right] \qquad (13)$$

3 Yee, Warming and Harten [3] Algorithm

The Yee, Warming and Harten [3] algorithm, second order accurate in space, is specified by the determination of the numerical flux vector at $(i+½,j,k)$ interface. The implementation of the other numerical flux vectors is straightforward.

According to a finite volume formalism, the right and left cell volumes, as also the interface volume, to coordinate change, are defined by:

$$V_R = V_{i+1,j,k},\ V_L = V_{i,j,k} \text{ and } V_{int} = 0.5(V_R + V_L). \qquad (14)$$

The metric terms to this generalized coordinate system are defined as:

$$h_x = S_{x\_int}/V_{int},\ h_y = S_{y\_int}/V_{int},\ h_z = S_{z\_int}/V_{int} \text{ and } h_n = S/V_{int}, \qquad (15)$$

where $S_{x\_int} = n_x S$, $S_{y\_int} = n_y S$, $S_{z\_int} = n_z S$ are the Cartesian components of the flux area and S is the flux area, calculated as described in Maciel [8-10], as also the cell volumes.

The properties calculated at the flux interface are obtained either by arithmetical average or by Roe [11] average. In this work, Roe [11] average was used. The speed of sound at the flux interface is given by:

$$a_{int} = \sqrt{(\gamma - 1)\left[H_{int} - 0.5\left(u_{int}^2 + v_{int}^2 + w_{int}^2\right)\right]}, \qquad (16)$$

where H_{int}, u_{int}, v_{int} and w_{int} are calculated at the flux interface. The eigenvalues of the Euler equations, in the ξ direction, are given by:

$$U_{cont} = u_{int}h_x + v_{int}h_y + w_{int}h_z,\ \lambda_1 = U_{cont} - a_{int}h_n, \qquad (17)$$

$$\lambda_2 = \lambda_3 = \lambda_4 = U_{cont};\ \lambda_5 = U_{cont} + a_{int}h_n. \qquad (18)$$

The jumps of the conserved variables, necessary to the construction of the Yee, Warming and Harten [3] dissipation function, are given, for example, by:

$$\Delta\rho = V_{int}(\rho_R - \rho_L) \text{ and } \Delta(\rho u) = V_{int}\left[(\rho u)_R - (\rho u)_L\right]. \qquad (19)$$

The α vectors at the $(i+½,j,k)$ interface are calculated by the following manner:

$$\{\alpha_{i+1/2,j,k}\} = \left[R^{-1}\right]_{i+1/2,j,k}\{\Delta_{i+1/2,j,k}\overline{Q}\}, \qquad (20)$$

with:

$$\left[R^{-1}\right] = \begin{bmatrix} 0.5\left[\left((\gamma-1)/a_{int}^2\right)0.5q^2 + \phi/a_{int}\right] & -0.5\left[\left((\gamma-1)/a_{int}^2\right)u_{int} + h'_x/a_{int}\right] & -0.5\left[\left((\gamma-1)/a_{int}^2\right)v_{int} + h'_y/a_{int}\right] & -0.5\left[(\gamma-1)/a_{int}^2 w_{int} + h'_z/a_{int}\right] & 0.5(\gamma-1)/a_{int}^2 \\ 1 - \left((\gamma-1)/a_{int}^2\right)0.5q^2 & \left((\gamma-1)/a_{int}^2\right)u_{int} & \left((\gamma-1)/a_{int}^2\right)v_{int} & (\gamma-1)/a_{int}^2 w_{int} & -(\gamma-1)/a_{int}^2 \\ -\left(h'_y u_{int} + h'_z v_{int} + h'_x w_{int}\right) & h'_y & h'_z & h'_x & 0 \\ -\left(h'_z u_{int} + h'_x v_{int} + h'_y w_{int}\right) & h'_z & h'_x & h'_y & 0 \\ 0.5\left[\left((\gamma-1)/a_{int}^2\right)0.5q^2 - \phi/a_{int}\right] & 0.5\left[-\left((\gamma-1)/a_{int}^2\right)u_{int} + h'_x/a_{int}\right] & 0.5\left[-\left((\gamma-1)/a_{int}^2\right)v_{int} + h'_y/a_{int}\right] & 0.5\left[-(\gamma-1)/a_{int}^2 w_{int} + h'_z/a_{int}\right] & 0.5(\gamma-1)/a_{int}^2 \end{bmatrix}; \qquad (21)$$

$$\{\Delta_{i+1/2,j,k}\overline{Q}\} = \{\Delta\rho \quad \Delta(\rho u) \quad \Delta(\rho v) \quad \Delta(\rho w) \quad \Delta e\}^T,$$

defined, for example, by Eq. (19); (22)

$$q^2 = u_{int}^2 + v_{int}^2 + w_{int}^2; \qquad (23)$$

$$\phi = u_{int}h'_x + v_{int}h'_y + w_{int}h'_z; \qquad (24)$$

$$h'_x = h_x/h_n,\ h'_y = h_y/h_n \text{ and } h'_z = h_z/h_n. \qquad (25)$$

The Yee, Warming and Harten [3] dissipation function uses the right-eigenvector matrix of the normal to the flux face Jacobian matrix in generalized coordinates:

$$[R]=\begin{bmatrix} 1 & 1 & 0 & 0 & 1 \\ u_{int}-h'_x a_{int} & u_{int} & h'_y & h'_z & u_{int}+h'_x a_{int} \\ v_{int}-h'_y a_{int} & v_{int} & h'_z & h'_x & v_{int}+h'_y a_{int} \\ w_{int}-h'_z a_{int} & w_{int} & h'_x & h'_y & w_{int}+h'_z a_{int} \\ H_{int}-h'_x u_{int} a_{int}-h'_y v_{int} a_{int}-h'_z w_{int} a_{int} & 0.5q^2 & h'_x w_{int}+h'_z v_{int}+h'_y u_{int} & h'_y w_{int}+h'_x v_{int}+h'_z u_{int} & H_{int}+h'_x u_{int} a_{int}+h'_y v_{int} a_{int}+h'_z w_{int} a_{int} \end{bmatrix}. \quad (26)$$

Two options to the ψ_l entropy function, responsible to guarantee that only relevant physical solutions are to be considered, are implemented aiming an entropy satisfying algorithm:

$$\nu_l = \Delta t_{i,j,k}\lambda_l = Z_l \quad \text{and} \quad \psi_l = Z_l^2 + 0.25; \quad (27)$$

or:

$$\psi_l = \begin{cases} |Z_l|, & if\ |Z_l| \geq \delta_f \\ 0.5\left(Z_l^2+\delta_f^2\right)/\delta_f, & if\ |Z_l| < \delta_f \end{cases}, \quad (28)$$

where "l" varies from 1 to 5 (three-dimensional space) and δ_f assuming values between 0.1 and 0.5, being 0.2 the value recommended by Yee, Warming and Harten [3]. In the present studies, Eq. (28) was used to perform the inviscid numerical experiments and Eq. (27) was used to perform the viscous numerical experiments.

The $\tilde{g}$ function at the *(i+½,j,k)* interface is defined by:

$$\tilde{g}^l = 0.5\left(\psi_l - Z_l^2\right)\alpha^l, \quad (29)$$

with α^l being the lth component of the alpha vector (Eq. 20).

The g numerical flux function, which is a limited function to avoid the formation of new extrema in the solution and is responsible to the second order accuracy of the scheme, is determined by:

$$g^l_{i,j,k} = signal_l \times MAX\left(0.0; MIN\left(\left|\tilde{g}^l_{i+1/2,j,k}\right|, \tilde{g}^l_{i-1/2,j,k}\times signal_l\right)\right), \quad (30)$$

where $signal_l$ is equal to 1.0 if $\tilde{g}^l_{i+1/2,j,k} \geq 0.0$ and -1.0 otherwise.

The θ term, responsible to the artificial compression, which enhances the resolution of the scheme at discontinuities, is defined in Maciel [10]. The β parameter at the *(i+½,j,k)* interface, which introduces the artificial compression term in the algorithm, is given by the following expression:

$$\beta_l = 1.0 + \omega_l MAX(\theta^l_{i,j,k}, \theta^l_{i+1,j,k}), \quad (31)$$

in which ω_l assumes the following values: ω_1 = 0.25 (non-linear field), $\omega_2 = \omega_3 = \omega_4 = 1.0$ (linear field) and ω_5 = 0.25 (non-linear field). The numerical characteristic speed, φ_l, at the *(i+½,j,k)* interface, which is responsible to transport the numerical information associated to the g numerical flux function, is defined by:

$$\varphi_l = \begin{cases} \left(g^l_{i+1,j,k} - g^l_{i,j,k}\right)/\alpha^l, & if\ \alpha^l \neq 0.0 \\ 0.0, & if\ \alpha^l = 0.0 \end{cases}. \quad (32)$$

The entropy function is redefined considering φ_l and β_l: $Z_l = \nu_l + \beta_l\varphi_l$, and ψ_l is recalculated according to Eq. (27) or to Eq. (28). The Yee, Warming and Harten [3] dissipation function is specified by the following product:

$$\{D_{YWH}\}_{i+1/2,j,k} = [R]_{i+1/2,j,k}\left\{\left[\beta\left(g_{i,j,k}+g_{i+1,j,k}\right)-\psi\alpha\right]/\Delta t_{i,j,k}\right\}_{i+1/2,j,k}. \quad (33)$$

The convective numerical flux vector to the *(i+½,j,k)* interface is described by:

$$F^{(l)}_{i+1/2,j,k} = \left(E^{(l)}_{int}h_x + F^{(l)}_{int}h_y + G^{(l)}_{int}h_z\right)V_{int} + 0.5D^{(l)}_{YWH}, \quad (34)$$

with:

$$E_{int}^{(l)} = 0.5\left(E_R^{(l)} + E_L^{(l)}\right),\ F_{int}^{(l)} = 0.5\left(F_R^{(l)} + F_L^{(l)}\right) \text{ and } G_{int}^{(l)} = 0.5\left(G_R^{(l)} + G_L^{(l)}\right). \quad (35)$$

The explicit version of this scheme employs a dimensional splitting method, first order accurate, which divides the temporal integration in three steps, each one associated with a different spatial direction. Details can be found in Maciel [9-10]. The treatment of the viscous gradients present in the Navier-Stokes equations is described in detail in Maciel [8-10].

4 Hughson and Beran [4] Algorithm

The Hughson and Beran [4] algorithm, second order accurate in space, follows Eqs. (14) to (26). The next step consists in determining the g numerical flux function. This function has different definitions to non-linear fields (l = 1 and 5) and linear fields (l = 2 to 4). Details of the definition of this function are found in Maciel [10]. Once the g function is determined, Eqs. (27), ν_l term, and (28) are employed and the σ_l term at the *(i+½,j,k)* interface is defined:

$$\sigma_l = 0.5\left(\psi_l - Z_l^2\right). \quad (36)$$

The φ_l numerical characteristic speed at the *(i+½,j,k)* interface is defined by:

$$\varphi_l = \begin{cases} \sigma_l\left(g_{i+1,j,k}^l - g_{i,j,k}^l\right)/\alpha^l, & if\ \alpha^l \neq 0.0 \\ 0.0, & if\ \alpha^l = 0.0 \end{cases}. \quad (37)$$

The entropy function is redefined considering the φ_l term: $Z_l = \nu_l + \varphi_l$ and ψ_l is recalculated according to Eq. (28). The Hughson and Beran [4] dissipation function is constructed by the following product:

$$\{D_{HB}\}_{i+1/2,j,k} = [R]_{i+1/2,j,k}\left\{\left(\sigma\left(g_{i,j,k} + g_{i+1,j,k}\right) - \psi\alpha\right)/\Delta t_{i,j,k}\right\}_{i+1/2,j,k}. \quad (38)$$

The convective numerical flux vector of the Hughson and Beran [4] scheme is defined by:

$$F_{i+1/2,j,k}^{(l)} = \left(E_{int}^{(l)}h_x + F_{int}^{(l)}h_y + G_{int}^{(l)}h_z\right)V_{int} + 0.5D_{HB}^{(l)}, \quad (39)$$

with $E_{int}^{(l)}$, $F_{int}^{(l)}$ and $G_{int}^{(l)}$ determined by Eq. (35). The explicit version of this algorithm to perform the inviscid and viscous simulations uses dimensional splitting, described in Maciel [9-10]. The implementation of the viscous terms follows the same procedure as reported in section 3.

5 Turbulence Models

5.1 Model of Cebeci and Smith [6]

The problem of the turbulent simulation is in the calculation of the Reynolds stress. Expressions involving velocity fluctuations, originating from the average process, represent six new unknowns. However, the number of equations keeps the same and the system is not closed. The modeling function is to develop approximations to these correlations. To the calculation of the turbulent viscosity according to the Cebeci and Smith [6] model, the boundary layer is divided in internal and external.

Initially, the (ν_w) kinematic viscosity at wall and the ($\tau_{xy,w}$) shear stress at wall are calculated. After that, the (δ) boundary layer thickness, the (δ_{LM}) linear momentum thickness and the (Vt_{BL}) boundary layer tangential velocity are calculated. So, the (N) normal distance from the wall to the studied cell is calculated. The N^+ term is obtained from:

$$N^+ = \sqrt{\mathrm{Re}}\sqrt{\tau_{xy,w}/\rho_w}\ N/\nu_w\,, \quad (40)$$

where ρ_w is the wall density. The van Driest damping factor is calculated by:

$$D = 1 - e^{\left(-N^+\sqrt{\rho/\rho_w}\,\mu_w/\mu/A^+\right)}, \quad (41)$$

with $A^+ = 26$ and μ_w is the wall molecular viscosity. After that, the (dVt/dN) normal to the wall gradient of the tangential velocity is calculated and the internal turbulent viscosity is given by:

$$\mu_{Ti} = \mathrm{Re}\,\rho(\kappa ND)^2\, dVt/dN\,, \qquad (42)$$

where κ is the von Kárman constant, which has the value 0.4. The intermittent function of Klebanoff is defined in Maciel [9-10]. With it, the external turbulent viscosity is calculated by:

$$\mu_{Te} = \mathrm{Re}(0.0168)\rho Vt_{BL}\delta_{LM}\, g_{Kleb}\,. \qquad (43)$$

Finally, the turbulent viscosity is chosen from: $\mu_T = MIN(\mu_{Ti}, \mu_{Te})$.

5.2 Model of Baldwin and Lomax [7]

To the calculation of the turbulent viscosity according to the Baldwin and Lomax [7] model, the boundary layer is again divided in internal and external. In the internal layer,

$$\mu_{Ti} = \rho l_{mix}^2 \|\omega\| \text{ and } l_{mix} = \kappa N\left(1 - e^{-N^+/A_0^+}\right). \qquad (44)$$

In the external layer,

$$\mu_{Te} = \rho\alpha C_{cp} F_{wake} F_{Kleb}(N; N_{\max}/C_{Kleb})\,, \qquad (45)$$

with F_{wake} and F_{max} defined in Maciel [9-10].

The constant values are: $\kappa = 0.4$, $\alpha = 0.0168$, $A_0^+ = 26$, $C_{cp} = 1.6$, $C_{Kleb} = 0.3$ and $C_{wk} = 1$. F_{Kleb} is the intermittent function of Klebanoff defined by the Baldwin and Lomax [7] model in Maciel [9-10], $\|\omega\|$ is the magnitude of the vorticity vector and U_{dif} is the maximum velocity value in the boundary layer case. To free shear layers,

$$U_{dif} = \left(\sqrt{u^2 + v^2 + w^2}\right)_{\max} - \left(\sqrt{u^2 + v^2 + w^2}\right)_{N = N_{\max}}. \qquad (46)$$

6 Initial and Boundary Conditions

Values of freestream flow are adopted in all properties as initial condition, in the whole calculation domain, to the ramp physical problem (Jameson and Mavriplis [12], and Maciel [8-10, 13-14]).

The boundary conditions are basically of three types: solid wall, entrance and exit. These conditions are implemented in special cells named ghost cells and details of these implementations are found in Maciel [8-10, 13-14].

7 Results

Tests were performed in a microcomputer with processor AMD ATHLON XP 2600+, 1.91GHz, and 512 Mbytes of RAM memory. A reduction of four orders of magnitude in the value of the maximum residue in the field, considering all conservation equations, was adopted as convergence criterion. The configuration upstream and the configuration longitudinal plane angles were set equal to 0.0°. The ramp problem is a supersonic flow hitting a ramp with 20° of inclination. It originates a shock wave and an expansion fan. The ramp configuration is described in Fig. 1, in the xy plane. Its spanwise length is 0.25m.

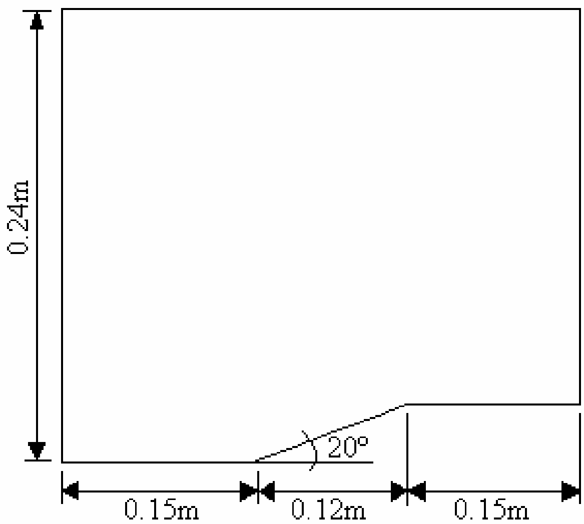

Figure 1. Ramp configuration at the xy plane.

A freestream Mach number of 5.0 (high supersonic flow) was adopted as initial condition to the inviscid and viscous laminar and turbulent simulations.

7.1 Inviscid Solutions

The mesh employed to the inviscid simulations has 61 points in the ξ direction, 60 points in the η direction and 10 points in the ζ direction. In finite volumes, this mesh is composed of 31,860 hexahedra and 36,600 nodes. Figure 1 and 2 shows the pressure contours obtained by the Yee, Warming and Harten [3] and the Hughson and Beran [4] schemes, respectively.

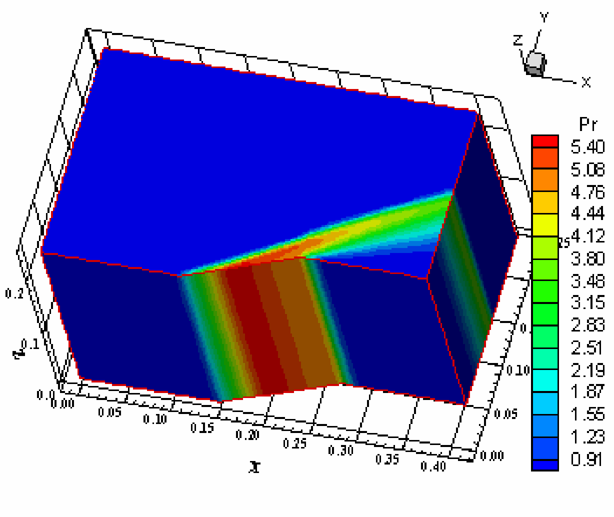

Figure 2. Pressure contours (YWH).

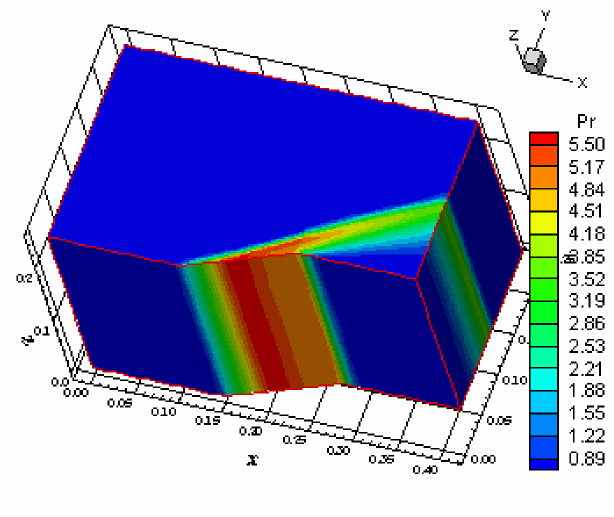

Figure 3. Pressure contours (HB).

Good symmetry and homogeneity properties are observed in both solutions. The pressure field generated by the Hughson and Beran [4] scheme is more severe than that generated by the Yee, Warming and Harten [3] scheme, characterizing the former as more critical, more conservative than the later.

Figure 4 presents the wall pressure distributions obtained bv both schemes at k = KMAX/2 (the middle of the ramp), where KMAX is the maximum number of points in the z direction (10 in this case). They are compared with the oblique shock wave and the Prandtl-Meyer expansion wave theories. Both solutions present a pressure oscillation at the ramp, which damages the quality of the solution. The width of the pressure plateau is not well captured by both schemes. Even the pressure after the expansion fan is bad captured by the schemes, presenting an under-shoot in this region.

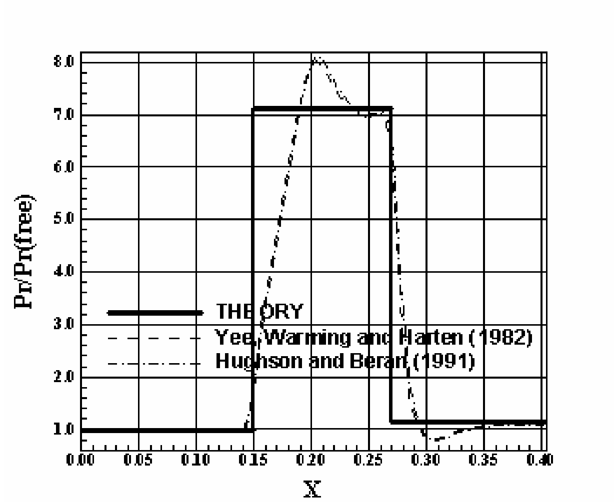

Figure 4. Wall pressure distributions.

7.2 Viscous Solutions

The mesh used in the viscous simulations has 37,260 hexahedra and 42,700 nodes. This mesh is equivalent, in finite differences, of being composed of 61 points in the ξ direction, 70 points in the η direction and 10 points in the ζ direction. An exponential stretching of 10% in the η direction was employed. The Reynolds number was estimated in $4x10^5$, to a flight altitude of 20,000m and l = 0.0437m, based on Fox and McDonald [15].

7.2.1 Laminar Results

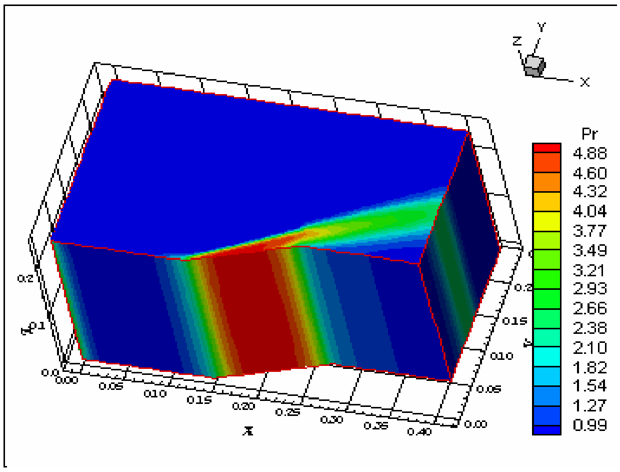

Figure 5. Pressure contours (YWH-L).

The laminar results presents the pressure contours obtained by the Yee, Warming and Harten [3] and the Hughson and Beran [4] algorithms described in Figs. 5 and 6. As can be observed, good symmetry characteristics and homogeneity properties are observed. The shock wave is well captured in both solutions and the Hughson and Beran [4] scheme again yields the most severe pressure field, characterizing it as the most conservative scheme.

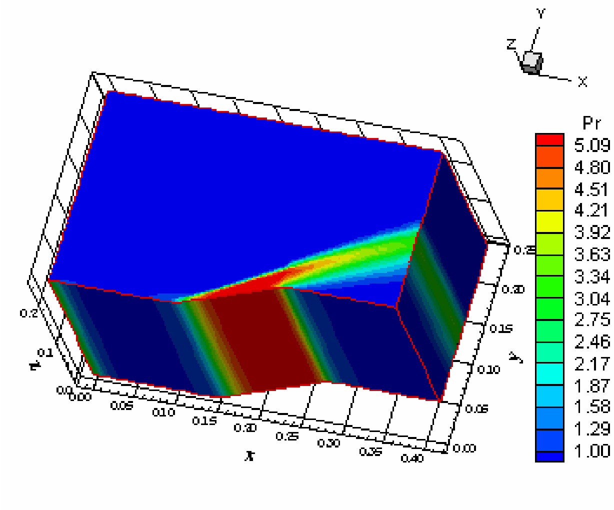

Figure 6. Pressure contours (HB-L).

7.2.2 *Cebeci and Smith [6] Results*

Figures 7 and 8 exhibit the pressure contours obtained by the Yee, Warming and Harten [3] and by the Hughson and Beran [4], respectively, using the Cebeci and Smith [6] turbulence model. As can be noted the Hughson and Beran [4] scheme is again the most conservative, presenting the most severe pressure field.

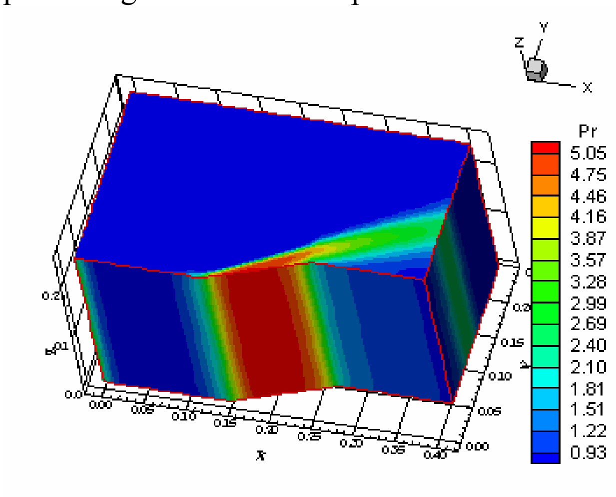

Figure 7. Pressure contours (YWH-CS).

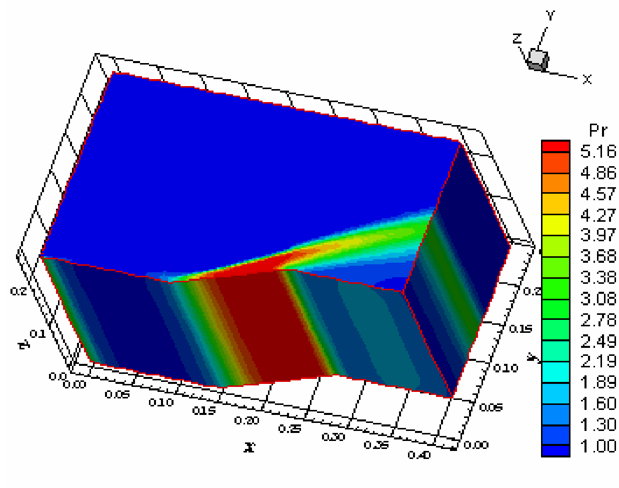

Figure 8. Pressure contours (HB-CS).

7.2.3 *Baldwin and Lomax [7] Results*

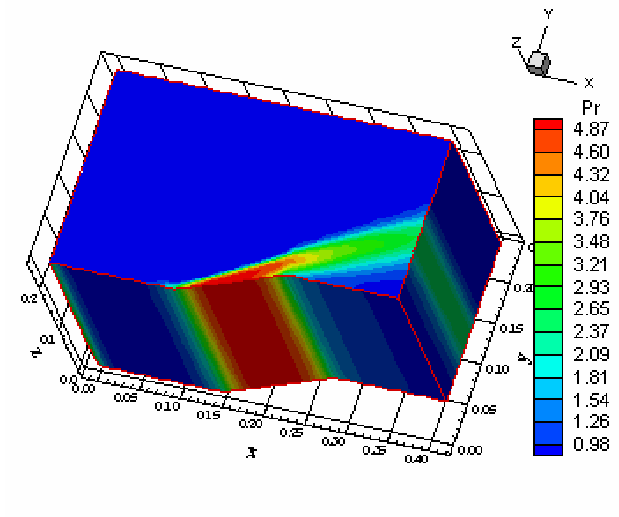

Figure 9. Pressure contours (YWH-BL).

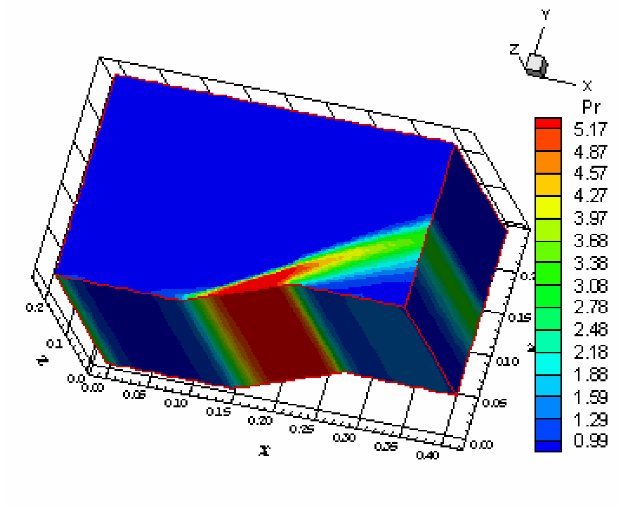

Figure 10. Pressure contours (HB-BL).

Figures 9 and 10 show the pressure contours obtained by the Yee, Warming and Harten [3] and the Hughson and Beran [4] TVD schemes, respectively, using the Baldwin and Lomax [7] turbulence model. The most severe pressure field is again obtained by the Hughson and Beran [4] algorithm.

7.2.4 Pressure Distributions and Shock Angle of the Oblique Shock Wave

Figure 11 exhibits the wall pressure distributions obtained by the Yee, Warming and Harten [3] algorithm in the laminar and turbulent cases. They are compared with the inviscid solution, the expected result due to boundary layer theory. The pressure distribution generated as using the Cebeci and Smith [6] model was the most severe.

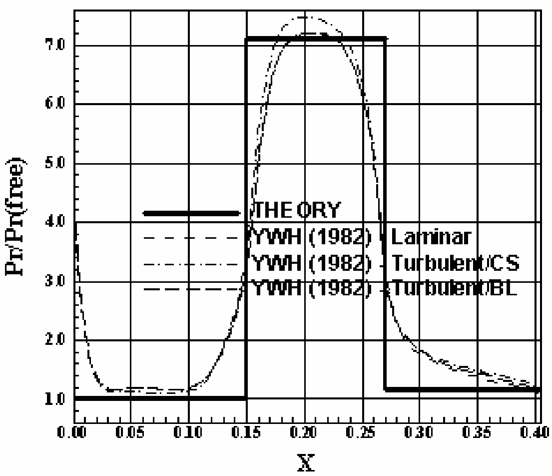

Figure 11. Wall pressure distributions (YWH).

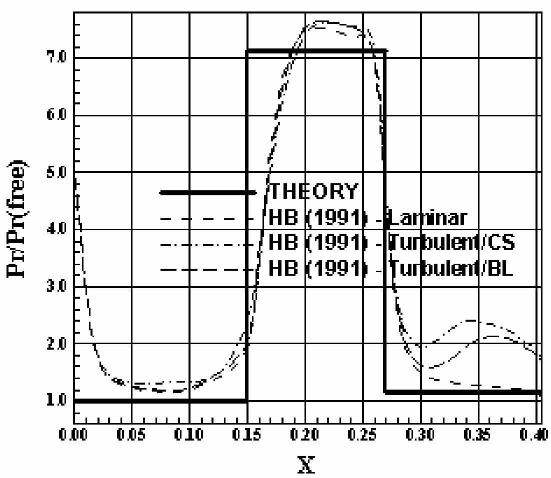

Figure 12. Wall pressure distributions (HB).

Figure 12 shows the wall pressure distributions obtained by the Hughson and Beran [4] algorithm in the laminar and turbulent cases. The pressure distribution generated as using the Baldwin and Lomax [7] model was the most severe. As conclusion, the pressure distributions generated by the Hughson and Beran [4] scheme are more severe.

One way to quantitatively verify if the solutions generated by each scheme are satisfactory consists in determining the shock angle of the oblique shock wave, β, measured in relation to the initial direction of the flow field. Anderson [16] (pages 352 and 353) presents a diagram with values of the shock angle, β, to oblique shock waves. The value of this angle is determined as function of the freestream Mach number and of the deflection angle of the flow after the shock wave, ϕ. To the ramp problem, ϕ = 20º (ramp inclination angle) and the freestream Mach number is 5.0, resulting from this diagram a value to β equals to 30.0º. Using a transfer in Figures 2, 3, 5 to 10, considering the xy plane, it is possible to obtain the values of β to each scheme, as well the respective errors, shown in Tab. 1, to each case. As can be observed, the best scheme was the Yee, Warming and Harten [3] one, using the Cebeci and Smith [6] model, with a percentage error of 0.33%. Moreover, the minimum errors were due to the Yee, Warming and Harten [3] scheme.

Table 1. Values of the shock angle and errors.

Algorithm	Case	β	Error (%)
Yee, Warming and Harten [3]	Inviscid	28.8	4.00
	Visc./Lam.	29.6	1.33
	Visc./CS	30.1	0.33
	Visc./BL	29.0	3.33
Hughson and Beran [4]	Inviscid	28.5	5.00
	Visc./Lam.	29.1	3.00
	Visc./CS	29.3	2.33
	Visc./BL	29.0	3.33

9 Conclusions

The present work performs comparisons between the Yee, Warming and Harten [3] and the Hughson and Beran [4] algorithms in the solution of inviscid and laminar and turbulent viscous flows in three-dimensions. The Euler and the Navier-Stokes equations, on a finite volume context and using a structured spatial discretization, are solved. The algorithms to perform numerical experiments are of TVD flux difference splitting type, second order accurate in space. A dimensional splitting method, first order accurate, is used to time integration. The physical problem of the supersonic flow along a ramp is studied. Turbulence is taking into account considering two turbulence models, namely: the Cebeci and Smith [6] and the Baldwin and Lomax [7] algebraic ones.

The results have demonstrated that the Hughson and Beran [4] scheme yields more severe pressure fields in all cases, characterizing this scheme as more conservative and indicated to the project phase of aerospace vehicle development. On the other hand, the Yee, Warming and Harten [3] scheme, in all cases, was the most accurate, being recommended to a more advanced project phase, where more accurate results are important to estimate the levels of security of the systems.

References

[1] Kutler P. Computation of Three-Dimensional, Inviscid Supersonic Flows. *Lecture Notes in Physics* Vol. 41, pp. 287-374, 1975.

[2] Steger JL. Implicit Finite-Difference Simulation of Flow About Arbitrary Two-Dimensional Geometries. *AIAA Journal*, Vol. 16, No. 7, pp. 679-686, 1978.

[3] Yee HC, Warming RF and Harten A. A High Resolution Numerical Technique for Inviscid Gas-Dynamic Problems with Weak Solutions. *Lecture Notes in Physics*, Vol. 170, pp. 546-552. Springer Verlag, Berlin, 1982.

[4] Hughson MC and Beran PS. Analysis of Hyperbolic Blunt-Body Flows Using a Total Variation Diminishing (TVD) Scheme and the MacCormack Scheme. *AIAA 91-3206-CP*, 1991.

[5] Harten A. High Resolution Schemes for Hyperbolic Conservation Laws. *Journal of Computational Physics* Vol. 49, No. 2, pp. 357-393, 1983.

[6] Cebeci T and Smith AMO. A Finite-Difference Method for Calculating Compressible Laminar and Turbulent Boundary Layers. *Journal of Basic Engineering*, Trans. ASME, Series B, Vol. 92, No. 3, pp. 523-535, 1970.

[7] Baldwin BD and Lomax H. Thin Layer Approximation and Algebraic Model for Separated Turbulent Flows. *AIAA Paper 78-257*, 1978.

[8] Maciel ESG. Simulação Numérica de Escoamentos Supersônicos e Hipersônicos Utilizando Técnicas de Dinâmica dos Fluidos Computacional. *Doctoral Thesis*, ITA, São José dos Campos, SP, Brazil, 258p, 2002.

[9] Maciel ESG. Explicit and Implicit TVD and ENO High Resolution Algorithms Applied to the Solution of the Euler and the Laminar and Turbulent Navier-Stokes Equations in Three-Dimensions. *Engineering Applications of Computational Fluid Mechanics* (under revision), 2008.

[10] Maciel ESG. TVD Algorithms Applied to the Solution of the Euler and the Laminar and Turbulent Navier-Stokes in Three-Dimensions. *Engineering Applications of Computational Fluid Mechanics* (under revision), 2008.

[11] Roe PL. Approximate Riemann Solvers, Parameter Vectors, and Difference Schemes. *Journal of Computational Physics,* Vol. 43, No. 2, pp. 357-372, 1981.

[12] Jameson A and Mavriplis DJ. Finite Volume Solution of the Two-Dimensional Euler Equations on a Regular Triangular Mesh. *AIAA Journal* Vol. 24, No. 4, pp. 611-618, 1986.

[13] Maciel ESG. Solution of the Navier-Stokes Equations in the Three-Dimensional Space Using the MacCormack Algorithm – Part II. *Proceedings of the XVIII International Congress of Mechanical Engineering (XVIII COBEM)*. Ouro Preto, MG, Brazil, 2005.

[14] Maciel ESG. Relatório ao Conselho Nacional de Pesquisa e Desenvolvimento Tecnológico (CNPq) sobre as Atividades de Pesquisa Desenvolvidas no Terceiro Ano de Vigência da Bolsa de Estudos para Nível DCR-IF Referente ao Processo nº 304318/2003-5. *Report, National Council of Research and Technological Development (CNPq)*. Brazil, August, 52 p, 2006.

[15] Fox RW and McDonald AT. *Introdução à Mecânica dos Fluidos*. Ed. Guanabara Koogan, Rio de Janeiro, RJ, Brazil, 632p, 1988.

[16] Anderson JD. *Fundamentals of Aerodynamics*. McGraw-Hill, Inc., EUA, 563p, 1984.

Copyright Statement